Journal of Power Sources 195 (2010) 3215–3223

Contents lists available at ScienceDirect

Journal of Power Sources

journal homepage: www.elsevier.com/locate/jpowsour

A novel full-field experimental method to measure the local compressibility of gas diffusion media

Yeh-Hung Lai[a,*], Yongqiang Li[a], Jeffrey A. Rock[b]

[a] Electrochemical Energy Research Lab, GM R&D, Honeoye Falls, NY 14472, United States
[b] GM Powertrain, Honeoye Falls, NY 14472, United States

ARTICLE INFO

Article history:
Received 1 October 2009
Received in revised form
18 November 2009
Accepted 25 November 2009
Available online 2 December 2009

Keywords:
PEM fuel cell
Gas diffusion media
Compressibility
Durability
Membrane shorting
Digital image correlation

ABSTRACT

The gas diffusion medium (GDM) in a proton exchange membrane (PEM) fuel cell needs to simultaneously satisfy the requirements of transporting reactant gases, removing product water, conducting electrons and heat, and providing mechanical support to the membrane electrode assembly (MEA). Concerning the localized over-compression which may force carbon fibers and other conductive debris into the membrane to cause fuel cell failure by electronically shorting through the membrane, we have developed a novel full-field experimental method to measure the local thickness and compressibility of GDM. Applying a uniform air pressure upon a thin polyimide film bonded on the top surface of the GDM with support from the bottom by a flat metal substrate and measuring the thickness change using the 3-D digital image correlation technique with an out-of-plane displacement resolution less than 0.5 μm, we have determined the local thickness and compressive stress/strain behavior in the GDM. Using the local thickness and compressibility data over an area of 11.2 mm × 11.2 mm, we numerically construct the nominal compressive response of a commercial Toray™ TGP-H-060 based GDM subjected to compression by flat platens. Good agreement in the nominal stress/strain curves from the numerical construction and direct experimental flat-platen measurement confirms the validity of the methodology proposed in this article. The result shows that a nominal pressure of 1.4 MPa compressed between two flat platens can introduce localized compressive stress concentration of more than 3 MPa in up to 1% of the total area at various locations from several hundred micrometers to 1 mm in diameter. We believe that this full-field experimental method can be useful in GDM material and process development to reduce the local hard spots and help to mitigate the membrane shorting failure in PEM fuel cells.

1. Introduction

A proton exchange membrane (PEM) fuel cell stack is comprised of a series arrangement of repeating cell units, each of which consists of a membrane electrode assembly (MEA) where the electrochemical reaction takes place; two layers of gas diffusion media (GDM) for the distribution of the fuel and oxidant gases over the catalytic surfaces; and a bipolar plate which directs the fuel and oxidant gases from the inlet manifolds through a network of flow channels. During the fuel cell stack assembly process, these repeating cells are stacked together with intermediate seal gaskets and then compressed to provide adequate gas sealing, as well as to reduce contact resistances at the material interfaces. The GDM plays an important role in PEM fuel cells by (1) serving as a mechanical buffer layer between the membrane electrode assembly and the adjacent bipolar plates; (2) acting as a diffuser for the reactant gases traveling to the electrodes; (3) transporting the product water to the gas flow channels; (4) conducting electrons; and (5) transferring the heat generated at the MEA to the coolant within the bipolar plates. GDM is normally composed of porous non-woven carbon fiber paper or carbon fiber cloth fabricated through the traditional paper manufacturing process [1]. Many researchers have investigated the effect of GDM compression on electrical, thermal, and mass transport resistances within the bulk material and across the contact interfaces [1–9]. To minimize contact resistance, high contact pressure between the lands of reactant gas flow field and gas diffusion media is usually desired. However, these studies generally find that the optimal compression pressure needs to be determined by balancing its conflicting effect on GDM's porosity, diffusivity, permeability, electrical conductivity, and thermal conductivity.

Compared to the body of knowledge in fuel cell performance, GDM's role on the impact of fuel cell durability is still relatively poorly understood and a dearth of literature on this subject can be found. Ohmic shorting through PEM has been identified as one of the major failure modes in PEM fuel cells [10–12]. Membrane

* Corresponding author. Tel.: +1 585 624 6329; fax: +1 585 624 6680.
E-mail address: yeh-hung.lai@gm.com (Y.-H. Lai).

0378-7753/$ – see front matter © 2009 Elsevier B.V. All rights reserved.
doi:10.1016/j.jpowsour.2009.11.122

shorting not only can reduce the performance of fuel cells, but also leads to local heat generation in the vicinity of the short, causing membrane damage that can ultimately result in gas crossover failures in fuel cells. Because of the serious consequence of membrane shorting, there is great need to fundamentally understand its causes, devise tests to evaluate the material sets, and develop mitigation methods. Since GDM is electronically conductive and in direct contact with the MEA, it is generally believed that GDM plays an important role in membrane shorting, possibly through the intrusion of carbon fibers into the membrane. Recently, Mittelsteadt and Liu [13] have reported an experimental study on membrane shorting using non-operating single small-scale (50 cm^2 active area) fuel cell fixtures to measure the cell ohmic resistance under both compression-ramp mode at constant environmental condition and humidity cycling mode under constant compression. They found strong correlation in reducing fuel cell ohmic resistance with increasing compression pressure. They also found that membrane shorting can be mitigated with the use of mechanical buffering layers such as micro porous layers (MPL) and catalyst layers. Their result showed strong contribution from GDM to the membrane shorting behavior.

Until recently, relatively little attention has been paid to the characterization of GDM's mechanical behavior and its effect on fuel cell performance and durability. Mathias et al. [1] investigated GDM's compressive stress/strain relationship by measuring the compressive deflection while repeatedly ramping up and down the compressive pressure on a GDM specimen placed between two flat platens. It was found that GDM exhibit different unloading and reloading curves from the first loading curve, suggesting weakening of the material from the first loading. To characterize GDM's bending behavior, Mathias et al. also proposed the use of flexural tests such as ASTM D790 to determine the flexural modulus and flexural strength. Lai et al. [14] investigated the compression pressure between GDM and MEA over flowfield lands and channels using finite element method and found that fuel cells could lose significant compression pressure due to the hysteresis in GDM's compressive behavior. Using the compressive stress/strain data from the platen compression test, elastic flexural modulus from the four-point-bend flexural test, and transverse shear modulus from a punch-and-die test, Lai et al. [15] calculated the intrusion of GDM into the channel in a single land/channel geometry using the finite element method. Excellent agreement in intrusion between the model prediction and experimental measurement shows the usefulness of these test methods to characterize the mechanical behavior of GDM.

1.1. Overview of GDM's nominal compressive behavior

Before embarking on the investigation of GDM's local compressive properties and the associated experimental methods, it is useful to gain insight into its average compressive behavior on a larger length scale. Following the test method first proposed by Mathias et al. [1], a GDM specimen of 25.4 mm in diameter was die-cut and placed between two flat cylindrical steel platens also 25.4 mm in diameter. After the initial thickness was measured under a 35-kPa pressure, the compression was then ramped up using an MTS® loading frame at a ramp rate of 58 kPa s^{-1}. The compressive deflection was measured with two extensometers attached on the cylindrical platens near the GDM specimen. Compressive strain was then determined by the ratio of compressive deflection to the initial thickness. Since fuel cell membranes can experience significant swelling cycles from water uptake and release during fuel cell operations, causing the adjacent GDM and the fuel cell stack to experience compressive loading and unloading [14], it is necessary to capture GDM's loading/unloading behavior. Thus, our platen compression test was conducted with multiple loading and unloading cycles with an increasing peak pressure for each consecutive cycle.

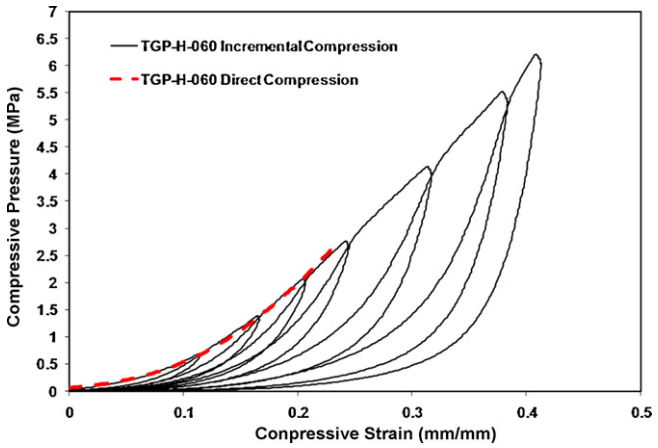

Fig. 1. Stress/strain curves of Toray™ TGP-H-060 under both incremental and direct platen compression loading.

Fig. 1 illustrates the typical compressive response of a non-woven carbon fiber-based GDM, Toray™ TGP-H-060 (Toray Industries, Inc., Tokyo, Japan). For convenience of discussion, we will trace the loading/unloading curves as the test proceeds in time. At a low compressive pressure, the GDM exhibits a relatively high compliance—an important feature for the GDM to act as a buffer layer to absorb the thickness variations in fuel cell components. As the compressive pressure is increased, its stiffness (defined as the force change per unit deflection change) also increases. During the subsequent unloading and reloading cycles, the GDM compression takes up paths below the original loading curve, suggesting that the material has suffered damages during the initial loading. The damage is believed to result from the rupture of carbon fibers and breakup of carbonized binders between the fibers. As the reloading surpasses the previous peaks, it exhibits a slight kink which then takes it onto the path of a virgin loading curve as can be connected by segments of the reloading curves between the neighboring peaks. A direct loading curve up to 2.75 MPa from a separate specimen is also plotted in Fig. 1, which shows excellent agreement with the virgin loading curve obtained from the incrementally loading/unloading method. As the compressive pressure is applied further along the virgin loading curve, additional damage can be created and the subsequent unloading will be on a different path than the previous ones.

Based on the compressive stress/strain curves in Fig. 1, one can easily find that GDM is the most compliant component in the repeating cell unit of a fuel cell stack. One of the direct consequences in an operating fuel cell where the membrane can repeatedly expand and contract significantly is the fluctuation of cell compression. For example, in a single fuel cell made of two layers of 180-μm Toray TGP-H-060 GDM, a 50-μm Nafion® N112 membrane (E. I. du Pont de Nemours, Wilmington, DE), two 10-μm catalyst layers, and two graphite flow field plates are held stationary upon an initial compression strain of 20% in GDM at about 2 MPa over lands after the cell is assembled. When the membrane experiences hydration from dry to 100%RH and back to dry, the 40% swing in the volumetric change [13] (hence the thickness change since membranes are generally well constrained in the in-plane directions by the electrodes, GDM, and the flow field plates), can induce a compression pressure swing from 2 to 3 MPa and back down to 0.75 MPa—a compression swing from 62.5% under-compression to 150% over-compression with respect to the targeted value of 2 MPa.

In addition to the over-compression resulting from the membrane hydration cycles of an operating fuel cell, another source of

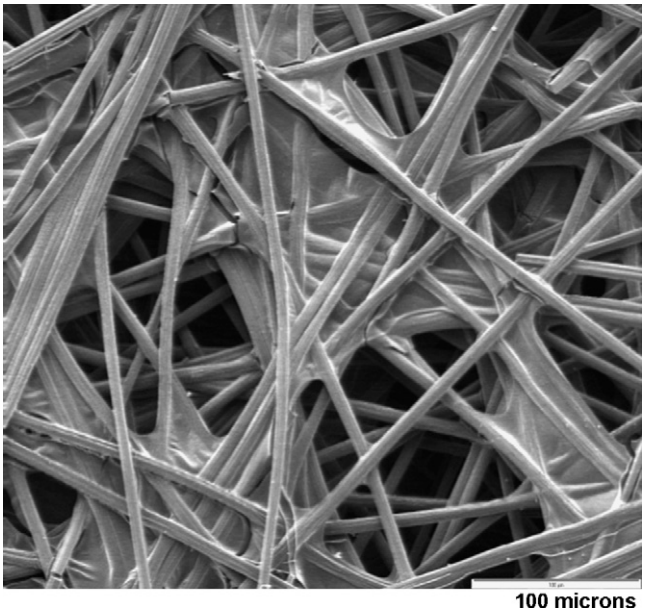

Fig. 2. A SEM micrograph of Toray™ TGP-H-060 GDM (without MPL coating).

over-compression over the membrane on a smaller length scale is from the heterogeneous nature in the non-woven carbon fiber substrate of the GDM. The SEM image of a Toray TGP-H-060, seen in Fig. 2, shows voids several hundred micrometers in size and criss-crossing fibers with binders in between. Since conglomerate of the former can form a soft spot within a GDM and those of the latter, a hard spot, we expect the hard spots to carry a much higher compressive pressure and potentially form high stress concentration points that may lead to membrane shorting.

Concerning with membrane shorting caused by GDM over-compression and its consequence on fuel cell durability, it is of great interest to develop a method to quantify and understand the local stress distribution within the GDM under the compression condition found in a fuel cell. Herein we propose a novel full-field high resolution experimental method to measure the thickness and compressibility distribution of GDM using the three-dimensional digital image correlation (3-D DIC) technique. The basic concept is to apply uniform air pressure over one side of the GDM which is sealed with a thin, flexible, and gas impermeable plastic film while supporting the other side of the GDM with a flat metal substrate. Using a full-field shape and displacement measurement technique such as 3-D DIC, the initial local thickness and the compressive deformation in GDM subjected to a prescribed air pressure history can be measured. From the air pressure and compressive deformation data, the local compressibility of the GDM can be determined. Simulating the platen compression with the local thickness and compressibility data over a large GDM area can then reveal the local compressive stresses in the GDM when it is compressed with a pair of rigid flat platens, similar to the compression of GDM by bipolar plates within a fuel cell. With the stress distribution determined, the severity and the nature of the stress concentration within the GDM can then be studied. In the following sections, we will describe in detail the experimental method and the conversion method from air pressure measurement to platen compression.

1.2. Overview of 3D-DIC technique

DIC was first used to investigate 2-D displacement and deformation by tracking features identified as different brightness values in charge-coupled device (CCD) camera images of an object in the early 1980s [16,17]. Using two cameras pointing at an object from different angles, 3-D DIC was developed in the 1990s [18,19] to measure the surface topology as well as the deformation of deformable bodies. Before testing a specimen, a random black and white speckle pattern is applied on its surface. Three-dimensional deformation history before and during the test are then recorded by simultaneously acquiring digital images of the surface with the two cameras. To translate the images into deformation history of the surface with a 3D-DIC program, an area of interest (AOI) is defined and a seed point is placed within the AOI in the image taken by the first camera before the test and a square pixel box (subset) is assigned around the seed point. Then the program searches in the image from the second camera taken at the same time for an area which matches the brightness profile of the subset box in the image from the first camera. After the match for the subset around the seed point is found, the program moves the seed point by a step size (smaller than the edge length of the subset) and conducts the same searching process for the subset surrounding the moved seed point. This process is repeated until the entire AOI is correlated and the reference 3-D surface is constructed through triangulation. After all images obtained during the test are correlated to the reference images, the deformation history of the surface is retrieved [20].

DIC provides full-field surface deformation information (for in-plane strains ranging from 0.1% to 500% and for out-of-plane displacement less than 1 μm) and is not limited by the physical size of the specimen as long as digital images can be recorded. It has become an accepted strain measurement technique and applications have been seen in measuring shape and deformation of wide and thin center-notched aluminum panels [21,22], large and heterogeneous deformation in polymeric foams [23,24] and deformation and crack opening displacement in mixed mode I/III fracture of aluminum [25]. In the area of PEM fuel cell technology, 2-D DIC was used to characterize the nonuniform deformation of membrane and MEA from a wet/dry cycle [26].

2. Experimental

A commercial DIC package including Vic-Snap® 2008, Vic-3D® 2007 by Correlated Solutions, Inc. (West Columbia, SC) and two 2448×2050 pixel^2, 14-bit CCD cameras by Prosilica, Inc. (Burnaby, BC) was used to capture and analyze digital images of the specimens. After calibration of the camera setup, the field-of-view was 24.4×23.3 mm^2, the baseline distance between the two cameras was found to be 210.7 mm and the angle between their optical axes 33.8°. The resolution for out-of-plane displacement measurements for this particular camera setup was determined to be below 0.5 μm.

A Toray TGP-H-060 GDM with 7 wt.% PTFE coated with 20 μm of proprietary micro porous layer (MPL) was used as a model GDM material in this study for test method development and validation purposes. GDM coupons, 58 mm in diameter as shown in Fig. 3, were cut to size with a steel rule die. The four notches around the edge of the sample were used for alignment purpose. A continuous circular piece of thin Kapton® polyimide film (71 mm in diameter and 12 μm thick, E. I. du Pont de Nemours, Wilmington, DE) coated with 25-μm pressure sensitive adhesive (3 M™ 467MP-200MP, St. Paul, MN) was bonded on the MPL side of each GDM coupon. It is believed that the thin polyimide film has low enough bending stiffness to easily conform to the surface of the deforming GDM under the settling pressure and beyond. Because of its very low modulus and relative small thickness, the pressure sensitive adhesive can easily seep into the pores of the GDM and is also believed not to change the mechanical response of the GDM. To create the speckle pattern for DIC measurement, the surface of the polyimide film was uniformly painted with a thin layer of Krylon® (Krylon Products

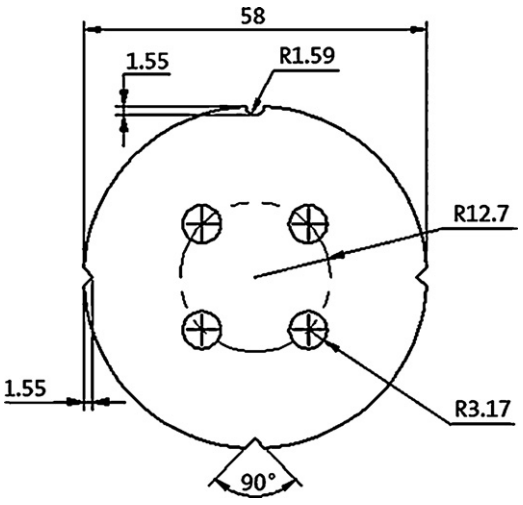

Fig. 3. Geometry of the GDM coupon (unit in mm). The four notches around the edge can be used to align the specimen with the test fixture. The four circular reference holes haloing the center of the coupon allow the portions of polyimide film suspended across them to adhere to the metal support under small air pressure.

Group, Cleveland, OH) flat white spray paint and then misted with flat dark spray paint of the same brand. This concludes the specimen fabrication and from herein a GDM specimen means a GDM coupon covered with a speckled polyimide film.

The experimental fixture and the response of a GDM specimen during a test are schematically shown in Fig. 4. The airtight fixture consists of a thick optical glass on the top and an aluminum substrate at the bottom. When a GDM specimen is laid on the substrate and clamped, an air pressure can be applied on the polyimide film therefore allowing compression test of the GDM coupon underneath. Owing to the porosity of the GDM and the small venting port built in the substrate, the air trapped under the polyimide film during the installation process can escape freely without building up a back pressure during a compression test. At the beginning of a test, under a settling pressure of 50 kPa (Fig. 4a), the portions of the polyimide film that span across the four reference holes were pressed and firmly bonded onto the substrate. During the test when the air pressure was ramped up and down, the sample surface deformed nonuniformly because of the gradient in compressibility across GDM (Fig. 4b). During the entirety of a test, the

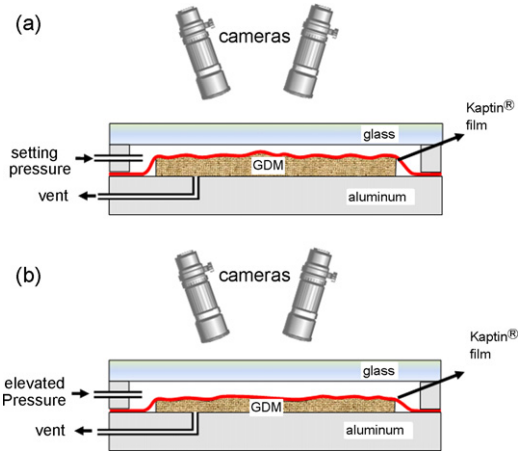

Fig. 4. The working concept of measuring full-field nonuniform thickness and compressibility of GDM using 3-D DIC. Enclosed in an airtight chamber and sealed with a thin polyimide film from the top, the GDM can be compressed with air pressure: (a) when a small settling pressure is applied at the beginning of the test; (b) under an elevated pressure.

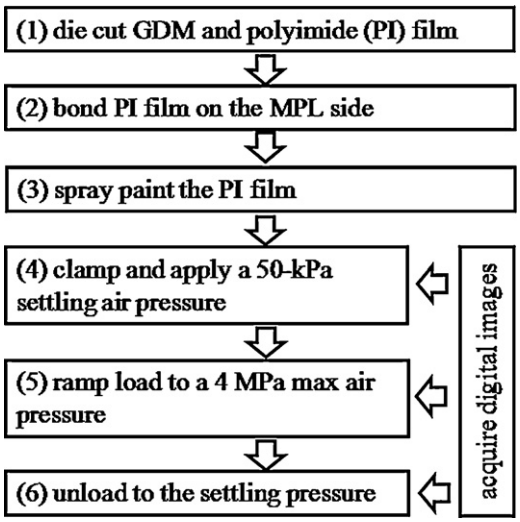

Fig. 5. Flowchart of the experimental procedure.

3-D DIC system was used to capture the deformation history of the GDM specimen through the glass. At the beginning, a few redundant pairs of images were captured with Vic-Snap® 2008 when the specimen settled down at 50 kPa. One of the images would serve as the reference for subsequent deformation calculation. While the air pressure was ramped from 50 kPa to a maximum pressure of 4 MPa and then lowered back to 50 kPa, Vic-Snap® 2008 was used to automatically capture images and record the air pressure history at every other second. The flow chart in Fig. 5 outlines all of the important aspects of the procedure for sample preparation and testing process.

2.1. Data reduction and analysis

Fig. 6 outlines the data reduction (steps a–d) and analysis (steps I–V) procedures after the tests. The data reduction process can be divided into two stages: DIC processing of the images in Vic-3D® (steps a and b) and reduction in Tecplot® 360 (steps c and d, Tecplot, Inc. Seattle, WA) [27]. The data analysis can be further separated into two parts: thickness and compressibility distribution analyses (I–III), which generates the nonuniform characteristic information of the GDM, and the simulation of platen compression test using local compressive properties obtained with the air pressure compression tests (IV and V), which provides the stress

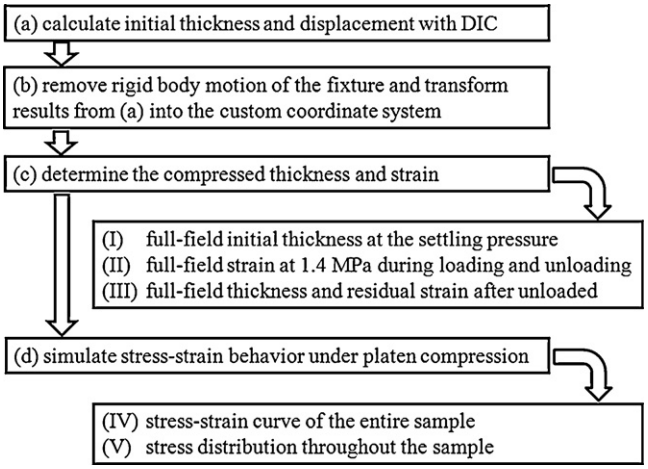

Fig. 6. Flowchart of the data reduction and analysis procedures.

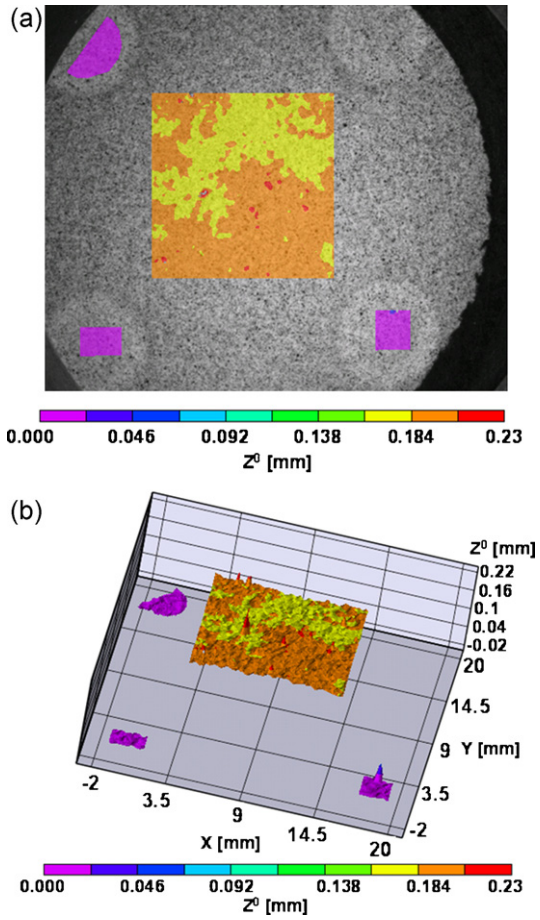

Fig. 7. Thickness data in Vic-3D 2007 illustrating the initial thickness of a TGP-H-060 sample under the settling pressure of 50 kPa. (a) 2-D contour plot overlaid on the digital image. The four reference holes, all in the $Z = 0$ plane, are visible around the perimeter of the field-of-view. (b) The same data plotted in 3-D illustrating the custom coordinate system with the z-axis parallel to the through thickness direction of the GDM sample.

distribution within the GDM under platen compression to reveal the "hard spots", i.e. areas producing higher than average compressive stresses.

In Vic-3D®, a pair of reference images in which the polyimide film across the four reference holes mostly adhered to the substrate were chosen from the first few images captured under the settling pressure. A primary area of interest (AOI) of 1000×1000 pixel^2 (in the present camera setup, 1 pixel equaled to 11.5 μm) was selected in the center of the field-of-view. Three reference AOIs were selected from three of the four reference holes (see Fig. 3). In the primary AOI, the subset size was 37 pixels and the step size was 5 pixels; in the reference AOIs, the subset size was also 37 pixels and the step size was 1 pixel. After correlation of all image pairs, displacements in the three reference AOIs within the reference holes were used to remove any rigid body motion of the fixture during the test. The entire dataset was then transformed into a custom coordinate system in which the center points of the three reference AOIs all fell in the $Z = 0$ plane and the X axis was parallel to one of the edges of the primary AOI. The AOIs and the contour plot of initial thickness measured at the settling pressure (50 kPa) are overlaid on the reference image in Fig. 7a. To illustrate the custom coordinate system, the contour plots are also shown in the 3-D space in Fig. 7b.

After the correlation, the dataset including X, Y (in-plane coordinates), Z_0 (initial thickness at 50 kPa), W (displacement in the through thickness direction) and p (air pressure) was exported into Tecplot® 360 for further reduction and analysis as in steps (c) and (d) in Fig. 6. Two new variables, the compressed thickness Z' and the compressive strain ε in the thickness direction were defined based on the initial thickness and the displacement at every data point in the field by the following equations,

$$Z'(X, Y) = Z_0(X, Y) + W(X, Y) \tag{1}$$

$$\varepsilon = \frac{Z' - Z_0}{Z_0} \tag{2}$$

All variables were measured or calculated locally and as pointed out earlier, the distance between neighboring data points (i.e. the step size used during the DIC analysis) was 5 pixels (57.7 μm). As this analysis procedure is performed from point to point throughout the AOI, the full field information of thickness and compressibility can be obtained.

In a PEM fuel cell, although the GDM compression varies from land to channel, the compressed thickness of the GDM is uniform across a land and from land to land. Therefore, the compression of GDM from land to land is more similar to the compression found in the platen compression test where the GDM is compressed between two rigid and parallel platens than in the air compression test. Consequently, given the local thickness and compressibility obtained from the air compression test with DIC, the nominal compressive pressure $\bar{\sigma}$ in the GDM when compressed to a uniform thickness of Z' using two platens can be determined by integrating the local pressure through all the data points within the AOI:

$$\bar{\sigma}(Z') = \frac{\sum_{i=1}^{N} p^i(Z')A^i}{A} \tag{3}$$

where p^i is the air pressure under which the ith point in the AOI reached the specified compressed thickness Z' during the air pressure compression test; A_i is the area represented by the ith point; N is the total number of data points that reached the specified compressed thickness, Z'; and A is the total area of the AOI. Note that this simulation of platen compression loading using air pressure compression results is effectively treating the GDM as a collection of individual springs with various lengths and spring behaviors. By accounting for the stress in each 'spring' for a given compressed thickness Z', we can map the stress distribution within the entire AOI. Interested readers are referred to Ref. [28] for details on this simulation process and its implementation in Tecplot® 360.

3. Results and discussions

The 1000×1000 pixel^2 AOI resulted in a data field with an edge lengths of 11.2 mm (the area represented by the data field is smaller than the AOI in the DIC analysis because bands half the edge length of the seed box were chopped off around the four boarders of the AOI), seeded with 194 data points at about 57.7-μm intervals in both in-plane directions. As will be seen shortly, for the TGP-H-060 sample, the 57.7-μm interval between neighboring data points is sufficient to distinguish areas of different thickness and compressibility in the GDM. Reducing the step size during the correlation process from 5 pixels to 1 pixel can enhance the sampling resolution to an interval of about 11.5 μm, but requires significantly more computation time.

The thickness distribution of the GDM under the 50-kPa settling pressure at the beginning and the end of the test after the air pressure was ramped up to 4 MPa and back down to 50 kPa is shown in the group of two contour and one histogram plots in Fig. 8. Significant thickness nonuniformity is found in the contour plots (Fig. 8a and b) before and after the 4 MPa air pressure load. The thickness contour plots reveal the spatial distribution of relatively thick and thin regions. From this plot, it is clear that the

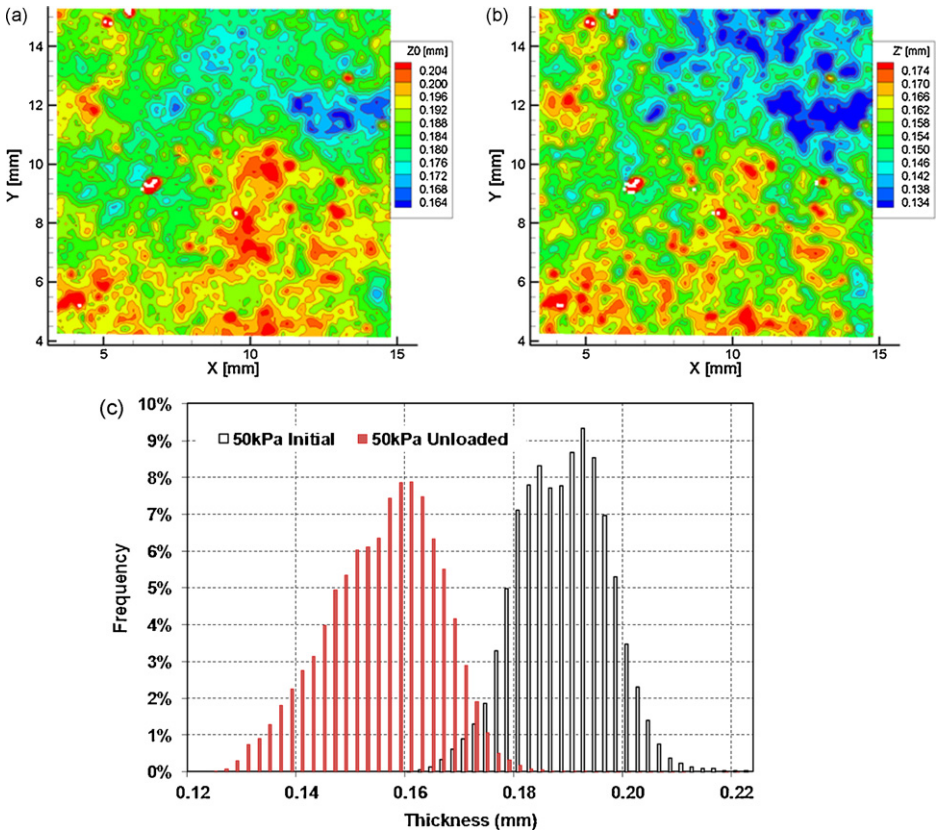

Fig. 8. The thickness distribution of the GDM under the settling pressure of 50 kPa before and after the 4 MPa pressure load; (a) and (b) are thickness contour plots before and after pressure load, respectively. (c) Histogram for Plots a and b.

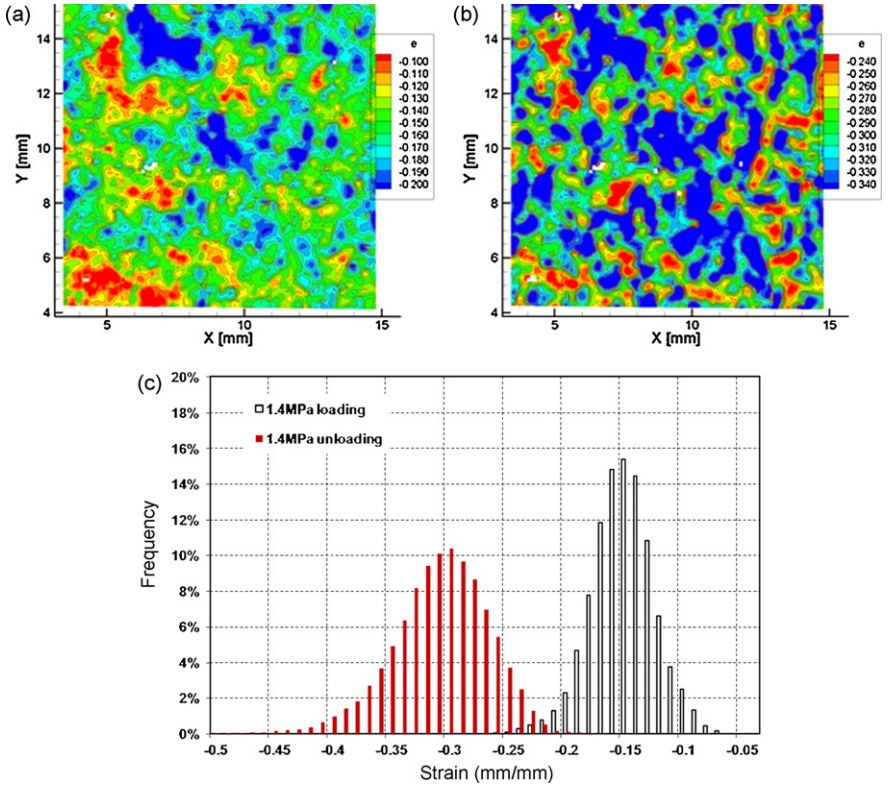

Fig. 9. Through thickness compressive strain in the GDM under 1.4 MPa pressure. (a) Contour plot of strain during loading from the settling pressure of 50 kPa to 1.4 MPa. (b) Contour plot of strain during unloading from 4 to 1.4 MPa. (c) Strain histograms for plots a and b.

57.7 μm interval between neighboring data points was sufficient to differentiate the thickness characteristics in the GDM sample. Within the AOI chosen in this study, the average thickness under the settling pressure before the 4 MPa pressure load was 187 μm with a standard deviation of 8 μm, a minimum thickness of 158 μm, and a maximum of 254 μm. Unloading from the 4 MPa pressure load, the average thickness becomes 155 μm, ranging from 120 to 220 μm, underscoring an overall permanent set of about 30 μm.

To investigate the compressibility distribution within the sample, the compressive strains in the sample under 1.4 MPa air pressure during pressure ramp up (loading) from 50 kPa and during pressure ramp down (unloading) from the peak pressure of 4 MPa are shown in a group of plots in Fig. 9. From both contour plots, one can see patches of stiffer (lower compressibility) as well as softer (higher compressibility) spots. It should be noted that the contour level scale has a 14% shift between the two plots. From the histogram of Fig. 9c, a wide range of compressive strain is seen in both cases. During loading, the compressive strain at 1.4 MPa has an average of 15.6%, ranging from 6.4% to 28.1% with a standard deviation of 2.7%. Unloading from the 4 MPa pressure load, the strain at 1.4 MPa air pressure has an average of 29.1%, ranging from 18% to 40% with a standard deviation of 3.9%. It is interesting to note that from the thickness and strain contour plots in Figs. 8 and 9, we do not find direct correlation between the compressibility and thickness. In this study, we find that the average in-plane principal strains in the polyimide film measured by DIC are less than 0.09% when the GDM is compressed by 15%. The negligible in-plane strain in a very thin film suggests that the GDM has a very low transverse Poisson's ratio and does not expand in-plane as it is compressed in the through thickness direction. The result also confirms that the polyimide film does not impede the deformation of GDM and the deflection at the surface of polyimide film should be solely a result of the response of the underlying GDM sample.

Fig. 10 illustrates the residual strain contour and histogram plots after unloading to 50 kPa from 4 MPa, where a wide distribution of residual compressive strain from 9% to 30% is seen. The average residual strain is 17.7% with a standard deviation of 3%.

From the results discussed in Figs. 8–10, significant nonuniform thickness and compressive properties are found within the GDM even for a relatively small area of 11.2 mm × 11.2 mm. The hard and soft spot distribution appear to be random. It was further observed that the nonuniformity remained throughout the loading and unloading process. It is obvious that these local features cannot be properly captured with the conventional platen compression test. Since the stress distribution in the GDM subjected to flat-platen compression is the most relevant to the membrane shorting problems within a fuel cell, we proceed to construct the compressive stress distribution of GDM between two flat platens with the already available local thickness and compressibility data. Using Eq. (3) and the process outlined in Section 2.1, stress–strain curves of the Toray TGP-H-060 based GDM under a simulated platen compression test can be constructed.

Fig. 11 illustrates the comparison of the simulated stress–strain curves based on air compression tests of three GDM samples with those obtained from actual platen compression tests of 25.4 mm-diameter samples using an MTS® loading frame. Four samples were tested in the platen compression test, from which average stress/strain data are plotted with the horizontal error bars representing the measured strain range. For convenience, only direct compression curves are shown and compared. It should be noted that a maximum simulated stress of 2.5 MPa is used as a cut-off point for the stress/strain simulation using the DIC data since an increasing number of points within the AOI required more pressure than the maximum air pressure of 4 MPa applied in the DIC

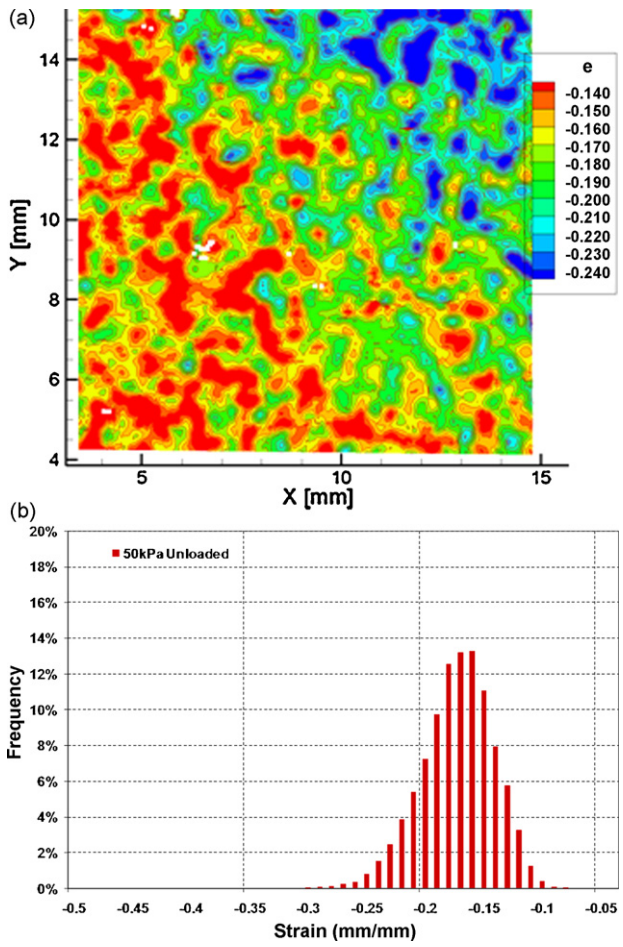

Fig. 10. Residual strain at 50 kPa after unloading from the peak pressure of 4 MPa. (a) Residual strain contour plot. (b) Residual strain histogram.

testing to be compressed to the common thickness corresponding to higher simulated stresses, defeating the spirit of Eq. (3). Generally, good agreement in the stress/strain data between the actual MTS tests and the simulation is seen in Fig. 11, though the deviation between the two groups of curves increases slightly at higher stress/strain levels. The increasing discrepancy at higher strain is

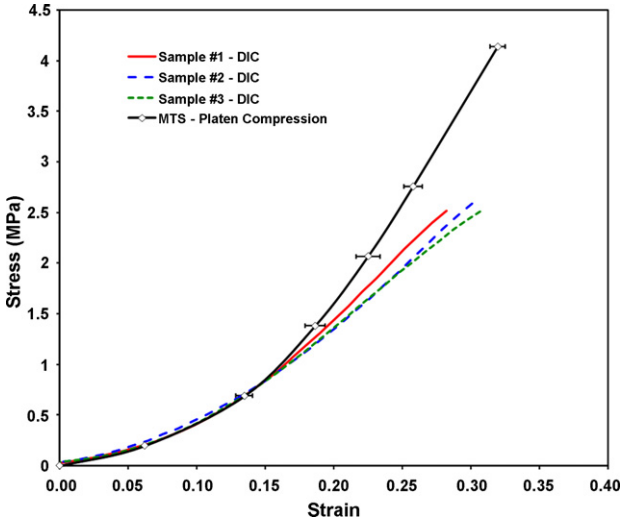

Fig. 11. The comparison of stress-strain curves from actual platen compression tests and the numerical construction with DIC local compressibility and thickness data.

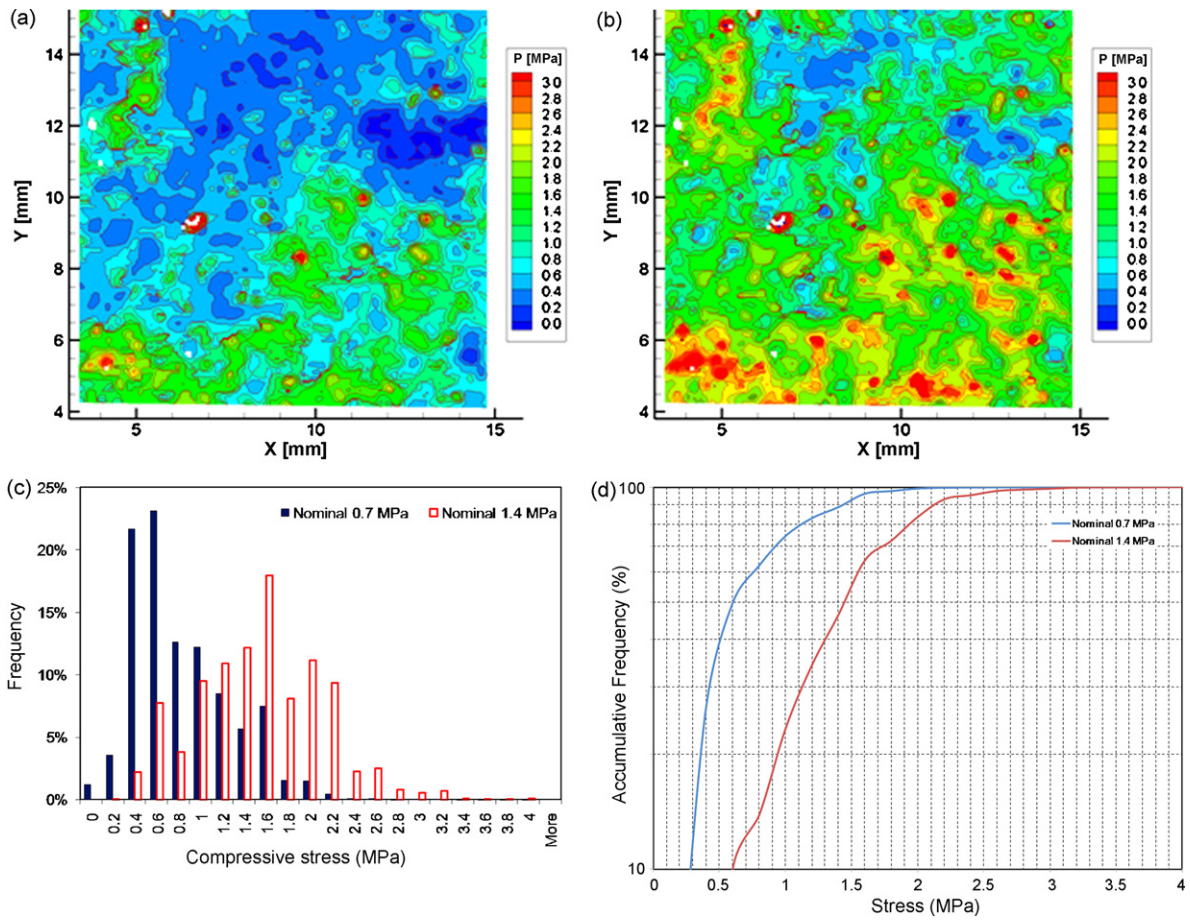

Fig. 12. Compressive stresses in the GDM subjected to simulated platen compression. (a) Stress contour plots in the GDM under a nominal compressive stress of 0.7 MPa. (b) Stress contour plots in the GDM under a nominal compressive stress of 1.4 MPa. (c) Stress histogram of contour plots a and b. (d) Accumulated frequency plots.

currently under investigation. However, the agreement in the nominal stress/strain comparison between the two groups suggests that the simulation is valid and that the result can be used to investigate the severity of stress concentration within the GDM under fuel cell compression condition.

To help understand the compressive stress distribution and the severity of stress concentration in the GDM under platen compression, the stress contour and histogram plots at two representative nominal stresses, 0.7 and 1.4 MPa, are investigated. In the case of 0.7 MPa shown in Fig. 12a, one can find significantly higher stresses in the lower half of the contour plots with a few spots exceeding 3 MPa. In the case of 1.4 MPa in Fig. 12b, both the number and the size of the spots that exceed 3 MPa increase, suggesting the increasing chance of mechanical damage to the MEA from those hard spots in the GDM. In the 0.7 MPa case, the hard spots exceeding 3 MPa are several hundred micrometers in diameter, however, in the 1.4 MPa case, the spots exceeding 3 MPa increase the size to about 1–2 mm.

Fig. 12c and d shows the stress histogram and cumulated frequency of both 0.7 and 1.4 MPa cases. In the 0.7 MPa case, the minimum stress is zero and the maximum stress is 3.2 MPa. About 1% of the total area has a stress exceeding 2 MPa or a stress concentration factor of about 3. In the 1.4 MPa case, the minimum stress is 0.4 MPa and the maximum is 4 MPa. About 1% of the total area has a stress exceeding 3 MPa. Since a typical automotive fuel cell system requires several hundred thousand cm^2 of active area, the seemingly small percentage of high stress concentration points can quickly amount to a significant area of high stress and pose a threat to fuel cell's durability.

4. Conclusions

Concerning the localized high compression from the GDM which may force carbon fibers and other conductive debris into the membrane to cause fuel cell failure by electronically shorting through the membrane, we have developed a novel full-field experimental method to measure the local thickness and compressibility of GDM. Applying a uniform air pressure upon a thin polyimide film bonded on the top surface of the GDM with support from the bottom by a flat metal substrate and measuring the thickness change using the 3-D digital image correlation technique, we have determined the local thickness and compressive stress/strain behavior in the Toray TGP-H-060 based GDM. The results showed that GDM have significant random disparity in both thickness and compressive property within an 11.2 mm × 11.2 mm area. Nearly 100 μm variation in thickness at a small settling pressure of 50 kPa was found within this area of interest with an initial average thickness of 187 μm. When compressed to 1.4 MPa air pressure, compressive strain ranged from 6.4% to 28.1%, showing evidence of soft and hard spots. Large residual strains and variations resulting from the unloading from 4 MPa suggest the damage within the GDM was also nonuniform.

Using the local thickness and compressibility data, the nominal compressive response of the Toray TGP-H-060 based GDM subjected to uniform thickness compression by flat platens was constructed numerically. Good agreement in the nominal stress/strain curves from the numerical construction and direct experimental flat-platen measurement confirms the validity of the methodology proposed in this article. The result shows that when

subjected to flat-platen compression, a nominal compression of 0.7 MPa can introduce a localized compressive stress higher than 2 MPa for up to 1% of the area of interest. These hard spots had the size from several hundred micrometers to 2 mm. To balance the need for lower ohmic contact resistance in the fuel cell by increasing compression pressure while decreasing the local GDM compressive stress for reduced membrane shorting and longer fuel cell durability, it is important to develop and use GDM with uniform thickness and compressibility to reduce the stress concentration. We believe this novel experimental method can be a useful tool in the material selection and development for both fuel cell system integrators as well as GDM suppliers.

Acknowledgements

The authors would like to thank Chunxin Ji, Mike Budinski, and Adam Cook for the help on the compression test using the flat-platen and providing images for this articles; Carl Marsiglio for the help in designing the compression fixture for the DIC test; and David Dillard, Mike Ellis, Scott Case, Gerald Fly, and Po-Ya Chuang for valuable discussions. Technical support on the DIC received from Micah Simonsen and Xiaodan Ke of Correlated Solutions, Inc. is also greatly appreciated.

References

[1] M. Mathias, J. Roth, J. Fleming, W. Lehnert, in: W. Vielstich, A. Lamm, H. Gasteiger (Eds.), Handbook of Fuel Cells: Fundamentals, Technology and Applications, vol. 3, John Wiley & Sons, Ltd., 2003 (Chapter 46).
[2] W.-K. Lee, C.-H. Ho, J.W.V. Zee, M. Murthy, J. Power Sources 84 (1999) 45–51.
[3] S.-J. Lee, C.-D. Hsu, C.-H. Huang, J. Power Sources 145 (2005) 353–361.
[4] H.S. Chu, C. Yeh, F. Chen, J. Power Sources 123 (2003) 1–9.
[5] J. Ge, A. Higier, H. Liu, J. Power Sources 159 (2006) 922–927.
[6] J. Ihonen, M. Mikkola, G. Lindbergh, J. Electrochem. Soc. 151 (8) (2004) A1152–A1161.
[7] I. Nitta, T. Hottinen, O. Himanen, M. Mikkola, J. Power Sources 171 (1) (2007) 26–36.
[8] T. Hottinen, O. Himanen, S. Karvonen, I. Nitta, J. Power Sources 171 (2007) 113–121.
[9] Y. Zhou, G. Lin, A.J. Shih, S.J. Hu, J. Power Sources 163 (2007) 777–783.
[10] M. Fowler, R.F. Mann, J.C. Amphlett, B.A. Peppley, Roberge P R.R, in: W. Vielstich, A. Lamm, H. Gasteiger (Eds.), Handbook of Fuel Cells: Fundamentals, Technology and Applications, vol. 3, John Wiley & Sons, Ltd., 2003 (Chapter 50).
[11] A.B. LaConti, M. Hamdan, R.C. McDonald, in: W. Vielstich, A. Lamm, H. Gasteiger (Eds.), Handbook of Fuel Cells: Fundamentals, Technology and Applications, vol.3, John Wiley & Sons, Ltd., 2003 (Chapter 49).
[12] C.S. Gittleman, F.D. Coms, Y.H. Lai, in: M.M. Mench, E.C. Kumbur, T. Nejat Veziroglu (Eds.), Modern Topics in Polymer Electrolyte Fuel Cell Degradation, 2010.
[13] C.K. Mittelsteadt, H. Liu, in: A.W. Vielstich, H. Gasteiger, H. Yokokama (Eds.), Handbook of Fuel Cells: Advances in Electrocatalysis, Materials, Diagnostics and Durability, vol. 5 and 6, John Wiley & Sons, Ltd., 2009.
[14] Y.H. Lai, D.P. Miller, C. Ji, T.A. Trabold, Proceedings of FUELCELL2004. Second International ASME Conference on Fuel Cell Science, Engineering and Technology, Rochester, NY, 2004.
[15] Y.H. Lai, P. Rapaport, C. Ji, V. Kumar, J. Power Sources 184 (2008) 120–128.
[16] W.H. Peters, W.F. Ranson, Opt. Eng. 21 (1982) 427–432.
[17] M.A. Sutton, W.J. Wolters, W.H. Peters, W.F. Ranson, S.R. McNeil, Image Vis. Comput. 4 (1986) 143–150.
[18] P.F. Luo, Y.J. Chao, M.A. Sutton, W.H. Peters, Exp. Mech. 33 (1993) 123–132.
[19] P.F. Luo, Y.J. Chao, M.A. Sutton, Opt. Eng. 33 (1994) 981–990.
[20] Vic-3D® User's manual, Correlated Solutions, Inc. 2008.
[21] J.D. Helm, M.A. Sutton, S.R. McNeill, Opt. Eng. 42 (2003) 1293–1305.
[22] J.D. Helm, M.A. Sutton, S.R. McNeill, Opt. Eng. 42 (2003) 1306–1320.
[23] Y. Wang, A.M. Cuitino, Int. J. Solids Struct. 39 (2002) 3777–3796.
[24] H. Jin, W.-Y. Lu, S. Scheffel, T.D. Hinnerichs, M.K. Neilsen, Int. J. Solids Struct. 44 (2007) 6930–6944.
[25] M.A. Sutton, J. Yan, X. Deng, C.–S. Cheng, P. Zavattieri, Opt. Eng. 46 (2007), 051003.
[26] L.G. Hector Jr., Y.H. Lai, W. Tong, M.J. Lukitsch, J. Fuel Cell Sci. Technol. 4 (2007) 19–28.
[27] Tecplot User's Manual, Tecplot, Inc., 2008, http://www.tecplot.com.
[28] Y. Li, Dissertation, Virginia Polytechnic Institute and State University, Blacksburg, VA, 2008, pp. 93–97 and 121–124, http://scholar.lib.vt.edu/theses/available/etd-12052008-115807/.